Received: 13 September 2017 | Revised: 22 November 2017 | Accepted: 19 December 2017

DOI: 10.1111/psyp.13064

ORIGINAL ARTICLE

WILEY PSYCHOPHYSIOLOGY SPR SOCIETY FOR PSYCHOPHYSIOLOGICAL RESEARCH

Toward a reliable, automated method of individual alpha frequency (IAF) quantification

Andrew W. Corcoran[1,2] | **Phillip M. Alday**[2,3] | **Matthias Schlesewsky**[2] | **Ina Bornkessel-Schlesewsky**[2]

[1] Cognition and Philosophy Laboratory, Monash University, Melbourne, Victoria, Australia

[2] Centre for Cognitive and Systems Neuroscience, University of South Australia, Adelaide, South Australia, Australia

[3] Max Planck Institute for Psycholinguistics, Nijmegen, The Netherlands

Correspondence
A. W. Corcoran, Cognition and Philosophy Laboratory, Room E672, Menzies Building, 20 Chancellors Walk, Monash University, Clayton, VIC 3800, Australia.
Email: andrew.corcoran1@monash.edu

Funding information
University of South Australia Ehrenberg-Bass Institute for Marketing Science, Australian Government Research Training Program (RTP) scholarship (to A. W. C.), Australian Research Council Future Fellowship (FT160100437) (to I. B. S.)

Abstract

Individual alpha frequency (IAF) is a promising electrophysiological marker of inter-individual differences in cognitive function. IAF has been linked with trait-like differences in information processing and general intelligence, and provides an empirical basis for the definition of individualized frequency bands. Despite its widespread application, however, there is little consensus on the optimal method for estimating IAF, and many common approaches are prone to bias and inconsistency. Here, we describe an automated strategy for deriving two of the most prevalent IAF estimators in the literature: peak alpha frequency (PAF) and center of gravity (CoG). These indices are calculated from resting-state power spectra that have been smoothed using a Savitzky-Golay filter (SGF). We evaluate the performance characteristics of this analysis procedure in both empirical and simulated EEG data sets. Applying the SGF technique to resting-state data from $n = 63$ healthy adults furnished 61 PAF and 62 CoG estimates. The statistical properties of these estimates were consistent with previous reports. Simulation analyses revealed that the SGF routine was able to reliably extract target alpha components, even under relatively noisy spectral conditions. The routine consistently outperformed a simpler method of automated peak detection that did not involve spectral smoothing. The SGF technique is fast, open source, and available in two popular programming languages (MATLAB, Python), and thus can easily be integrated within the most popular M/EEG toolsets (EEGLAB, FieldTrip, MNE-Python). As such, it affords a convenient tool for improving the reliability and replicability of future IAF-related research.

KEYWORDS

alpha rhythm, EEG, individual alpha frequency, oscillation/time frequency analyses, posterior dominant rhythm, Savitzky-Golay filter

1 | INTRODUCTION

Alpha is the dominant rhythm in the human EEG, and its importance for cognitive processing has been recognized since Hans Berger's seminal work in the early 20th century (Berger, 1929; cf. Adrian & Matthews, 1934). Interindividual differences in the predominant frequency of alpha-band oscillations (i.e., individual alpha frequency; IAF) have been linked with variability in cognitive performance since the 1930s (see Vogel & Broverman, 1964; for a more recent review, see Klimesch, 1999). More recent research has revealed that IAF predicts performance on a variety of perceptual (e.g., Cecere, Rees, & Romei, 2015; Samaha & Postle, 2015) and cognitive (e.g., Bornkessel, Fiebach, Friederici, & Schlesewsky, 2004; Klimesch, Doppelmayr, & Hanslmayr, 2006) tasks. Individuals with a low IAF process information more slowly (Klimesch, Doppelmayr, Schimke, & Pachinger, 1996; Surwillo, 1961, 1963), and show reduced performance on memory tasks (Klimesch, 1999) and general intelligence measures (Grandy, Werkle-Bergner, Chicherio,

 © 2018 Society for Psychophysiological Research

Lövdén et al., 2013), in comparison to their high-IAF counterparts. IAF is a trait-like characteristic of the human EEG (Grandy, Werkle-Bergner, Chicherio, Schmiedek et al., 2013), which shows high heritability (Lykken, Tellegen, & Thorkelson, 1974; Malone et al., 2014; Smit, Wright, Hansell, Geffen, & Martin, 2006) and test-retest reliability (Gasser, Bächer, & Steinberg, 1985; Kondacs & Szabo, 1999; Näpflin, Wildi, & Sarnthein, 2007). However, IAF tends to decrease with age from young adulthood onward (Chiang, Rennie, Robinson, van Albada, & Kerr, 2011; Köpruner, Pfurtscheller, & Auer, 1984); hence, lifelong changes in IAF accompany the decline of many cognitive abilities in older adulthood (e.g., Hedden & Gabrieli, 2004; Salthouse, 2011). Taken together, this evidence highlights the utility of the IAF as a neurophysiological marker of general brain functioning (Grandy, Werkle-Bergner, Chicherio, Lövdén et al., 2013; Grandy, Werkle-Bergner, Chicherio, Schmiedek et al., 2013).

In addition to quantifying individual differences in the properties of the dominant alpha rhythm, IAF can also be used to derive individualized estimates of the canonical frequency bands beyond the alpha range (Klimesch, 2012). Such empirically driven approaches to frequency band definition have been proposed to sharpen the precision of frequency-domain analyses more generally (Klimesch, 2012). Indeed, using the IAF to distinguish subregions of the alpha band has revealed functional dissociations between lower- and higher-frequency alpha rhythms (e.g., Klimesch, 1997). However, despite the potential advantages of deploying the IAF as a reference point for various kinds of individualized spectral analysis, no clear consensus on the optimal method for quantifying IAF currently exists. This paper thus sets out to develop a rigorous, automated strategy for estimating two of the most widely reported indices of IAF: peak alpha frequency (PAF) and alpha frequency center of gravity (CoG). We begin by briefly describing some of the most common strategies for extracting these estimators and some of their attendant problems.

1.1 | Peak alpha frequency

IAF estimation typically depends on the delineation of a singular, prominent spectral peak within the alpha bandwidth (standardly defined as 8–13 Hz; Noachtar et al., 2004). In many cases, the PAF can be easily discerned upon visual inspection of the power spectral density (PSD) from eyes-closed resting-state EEG recorded over parieto-occipital sites. However, this strategy can be complicated by the presence of two (or more) alpha-band peaks (so-called split peaks; Chiang et al., 2011) or the lack of any obvious peak-like deviation from the characteristic $1/f$ scaling of background M/EEG spectral activity (the "inverse power law," Pritchard, 1992; see Figure 1). Under such circumstances, subjective PAF estimation may be prone to bias and inconsistency (Chiang et al., 2008), thus posing a significant challenge to replicability. While conservative approaches to PAF identification in the context of ambiguous spectral conditions may help to reduce bias, this may result in high rates of attrition (see, e.g., Bornkessel-Schlesewsky et al., 2015).

One approach for improving the objectivity, replicability, and (for larger data sets) practicality of PAF estimation is to implement an automated peak-detection algorithm. While this strategy does not solve the basic problem of deciding the criteria by which valid PAF estimates are discriminated from split peaks or spurious background fluctuations, it at least applies such criteria consistently across all subjects. Simple algorithms may, however, introduce new sources of bias. For instance, a basic routine that searches for local maxima within the alpha band may arbitrarily assign the PAF to the lower bound of the search window in the absence of any notable deviation from the inverse power law (since the highest power estimate will be the supremum found at the lowest frequency bin spanned by the window). A more sophisticated approach such as the first-derivative test (in which the first derivative of the PSD is searched for downward-going zero crossings; cf. Grandy, Werkle-Bergner, Chicherio, Schmiedek et al., 2013) avoids this problem, but is still incapable of distinguishing substantive peaks from split peaks or arbitrarily small deviations from background spectral activity. Such routines may therefore be too liberal with regard to the spectral features they classify as alpha peaks.

1.2 | Alpha-band center of gravity and reactivity

The alpha mean or CoG frequency (Klimesch, Schimke, Ladurner, & Pfurtscheller, 1990) has been proposed as an alternative method of IAF estimation that circumvents some of the difficulties posed by the absence of a dominant alpha peak (Klimesch, 1997; Klimesch, Schimke, & Pfurtscheller, 1993). This estimator computes a weighted average of the power contained within the alpha band, thus rendering a summary measure that is sensitive to the spectral distribution of alpha components. Given that the span and location of alpha-rhythm activity vary across individuals (Bazanova & Vernon, 2014), Klimesch and colleagues (1990) recommended computing the CoG using bespoke frequency windows designed to capture such variation. However, the definition of such individualized alpha-band windows (IAWs) poses a nontrivial challenge, and may rely on subjective assessments or arbitrary criteria (Bazanova & Vernon, 2014). One principled solution to this problem is to derive the IAW from reactivity-based contrasts between two conditions (e.g., eyes-closed vs. eyes-open resting states, Klimesch, 1999; pre- vs. peristimulus presentation, Goljahani et al., 2012). This approach is not immune to bias, however,

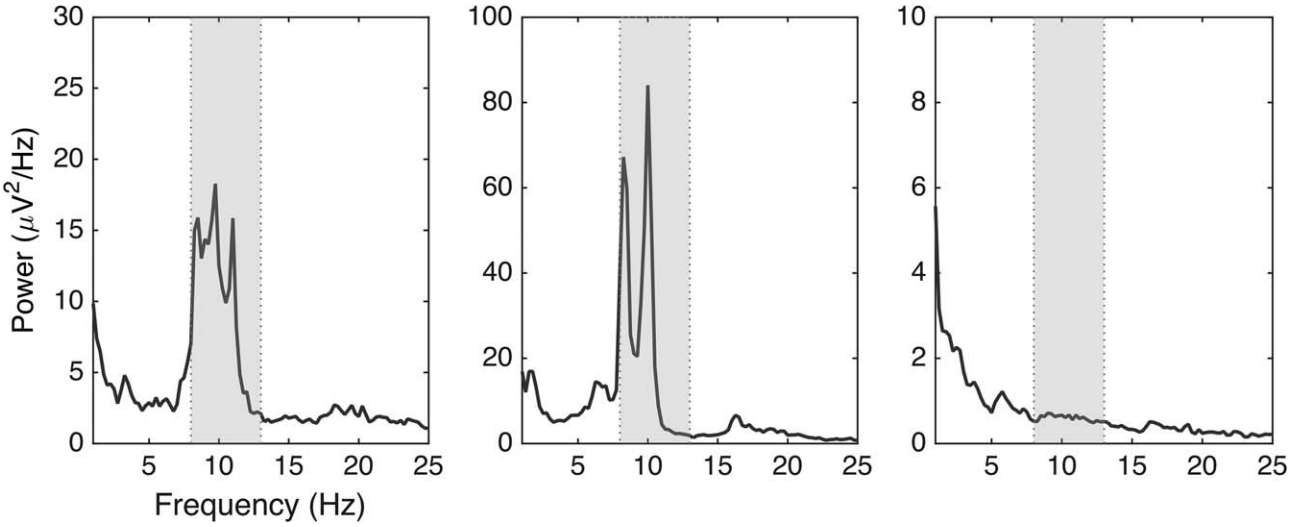

FIGURE 1 Empirical examples of problematic cases for peak alpha frequency identification. Standard alpha-band interval (8–13 Hz; Noachtar et al., 2004) indicated by shaded column. Left: Multiple peaks resolved within the alpha-band interval. Center: Split (bimodal) alpha peak. Right: No discernable alpha peak. Note differences in *y* axis scaling

since alpha rhythms are not always substantially attenuated by opening the eyes (Gaál, Boha, Stam, & Molnár, 2010; Kreitman & Shaw, 1965), and may only be partially attenuated (e.g., Klimesch et al., 2006)—or even enhanced (e.g., Rihs, Michel, & Thut, 2007)—during experimental tasks.

1.3 | Curve-fitting approaches to alpha-rhythm quantification

One promising approach to spectral peak quantification that avoids many of the issues highlighted above applies iterative curve-fitting techniques to parameterize the statistical properties of the PSD (e.g., Chiang et al., 2008; Lodder & van Putten, 2011). The practical utility of such methods is clearly apparent from their application to large *n* data sets (e.g., Chiang et al., 2011; van Albada & Robinson, 2013), while comparison of Lodder and van Putten's (2011) algorithm with human scorers revealed a high degree of estimator agreement. It is thus puzzling why such methods have not been taken up more broadly within the IAF literature (cf. Haegens, Cousijn, Wallis, Harrison, & Nobre, 2014, for a notable exception). One possibility is that investigators are generally unaware of these approaches, given that they have mostly been applied in the context of spectral modeling rather than IAF-focused research (indeed, neither Goljahani et al., 2012, nor Bazanova & Vernon, 2014, mention the existence of curve-fitting methods in their reviews of IAF estimation techniques). Alternatively, investigators may be put off by the perceived burden involved in accessing these programs (which we have been unable to locate online) and integrating them within existing analysis pipelines (which may not be compatible with such algorithms). We suggest then that one of the critical steps toward achieving a more widespread adoption of automated IAF estimation techniques is to make these tools openly available in formats that can be easily assimilated within popular methods of M/EEG analysis.

1.4 | Aims of the present study

In sum, common methodological approaches to IAF estimation are either (a) time consuming and vulnerable to inconsistencies arising from subjective evaluation, or (b) at risk of producing spurious or biased estimates under certain plausible spectral conditions. More recent innovations that address these problems via the application of sophisticated curve-fitting algorithms have so far found limited uptake within the broader IAF literature, perhaps on account of practical barriers pertaining to software access and implementation. Consequently, we sought to develop an automated method of alpha-band spectral quantification that provides fast, reliable, and easily replicated estimates of the resting-state IAF in two major programming languages: MATLAB (The MathWorks, Inc., Natick, MA) and Python. This goal is consistent with recent proposals to make the analysis of electrophysiological data as open, transparent, and amenable to replication as possible (Cohen, 2017).

2 | METHOD

Our approach aims to emulate Klimesch and colleagues' (1990) original attempt to characterize individual profiles of resting-state alpha-band activity by means of a relatively simple, nonparametric curve-fitting technique—the Savitzky-Golay filter (SGF). The basic strategy runs as follows: First we extract PSD estimates from preprocessed, fast

Fourier-transformed EEG signals. Second, we apply the SGF to smooth the PSD function and estimate its first- and second-order derivatives. Third, these derivatives are analyzed for evidence of a distinct spectral peak within the alpha-band region. Finally, the first derivative of the PSD is reanalyzed to locate the bounds of the IAW, from which the CoG is estimated. Our main focus here will be to assess the efficacy of this approach in the context of both empirical and simulated data. For a more rigorous account of the calculations implemented in the algorithm, see the Appendix.

It should be noted from the outset that our approach does not set out to discriminate fine-grained differences in alpha-band activity at the source level. Although recent research (e.g., Barzegaran, Vildavski, & Knyazeva, 2017; Haegens et al., 2014; van der Meij, van Ede, & Maris, 2016) has borne out earlier intuitions that alpha rhythms detected over posterior scalp regions comprise a mixture of overlapping oscillatory components (see Başar, 2012; Klimesch, 1999), our main concern here was to develop a method for deriving reliable summary estimates of the dominant alpha rhythm for analyses of interindividual differences in cognition (see Section 4.3 Limitations and Future Developments for further discussion).

2.1 | Savitzky-Golay smoothing and differentiation

The SGF is a least-squares polynomial curve-fitting procedure specifically designed to aid the detection of spectral peaks amid noisy conditions (Savitzky & Golay, 1964). The SGF has a number of properties that make it well suited to the task of smoothing PSD functions, not least of which is its capacity to render smoothed curves that conserve the height, width, position, area, and center of gravity of the underlying spectral structure (see Ziegler, 1981). SGFs work by centering a sampling window of length F_w on a portion of the input signal and computing the least-squares fit of a specified polynomial to each ith data point spanned by F_w. The window is then shifted one point along the input signal, and the polynomial fit recalculated accordingly. The center value of the polynomial fit is taken as the filter output at each iteration of the sliding window calculation, and these values are concatenated to render the smoothed estimate of the input function. For a more detailed treatment of the SGF and its technical performance properties, the interested reader is referred to Schafer (2011).

We propose using the SGF in order to attenuate random fluctuations in the PSD (and thus improve signal-to-noise ratio, SNR) without substantially distorting the spectral parameters of interest in IAF analysis. Eliminating such fluctuations should reduce the number of spurious local optima in the derivatives of the PSD, thus improving the overall accuracy and reliability of the first-derivative test. Conveniently, SGFs constitute optimal (or near optimal) differentiators (Luo, Ying, He, & Bai, 2005), and hence can be deployed to simultaneously estimate both the smoothed PSD and its derivative functions.

2.2 | Implementation

All functions developed in order to conduct the analyses reported here are open source and available (along with sample data sets, tutorial, and simulation materials) from <https://github.com/corcorana/restingIAF>. The following report focuses on the MATLAB implementation of the algorithm, which is dependent on the Signal Processing Toolbox. The pipeline (Figure 2) relies on MATLAB's *pwelch.m* implementation of Welch's modified periodogram method (Welch, 1967) to derive PSD estimates. This requires the selection of a sliding window function of length x, which determines the frequency resolution of the analysis. (Note that alternative methods of PSD estimation could be coupled with the SGF routine, but are not explored here.) The following parameters must also be specified in order to execute the algorithm (examples of what we consider to be reasonable values are outlined in Section 2.3.4 IAF Analysis Parameters):

- F_w, SGF frame width (longer = more smoothing; Bromba & Ziegler, 1981);
- k, SGF polynomial degree (higher = less smoothing/peak height attenuation; Press, Teukolsky, Vetterling, & Flannery, 1992);
- W_α, the domain of the PSD searched for evidence of peak activity;
- *minP*, the minimum power value that a local maximum must exceed to qualify as a peak candidate (defined as 1 *SD* above the power estimate predicted by a regression model of the log-transformed PSD);
- *pDiff*, the minimum proportion of peak height by which the highest peak candidate within W_α must exceed any competitors to be assigned as the PAF;
- *cMin*, the minimum number of channel estimates necessary for computing cross-channel averages.

Since channel spectra may be differentially contaminated by signal noise, our algorithm evaluates the relative "quality" of channelwise PAF estimates prior to cross-channel averaging. To this end, we extend the logic of the first-derivative test to extract second derivative estimates of the inflection points bounding the PAF. These points are used to define the area under the peak (in normalized power units), which is then divided by the frequency span of this area. The resulting quantity (Q value) thus affords an indication of the relative quality of the resolved peak in terms of how well its distributional characteristics conform to the ideal of a highly powered, less variable (i.e., narrower) peak (as opposed to broader and/or shallower counterparts). Within-subject channel estimates are

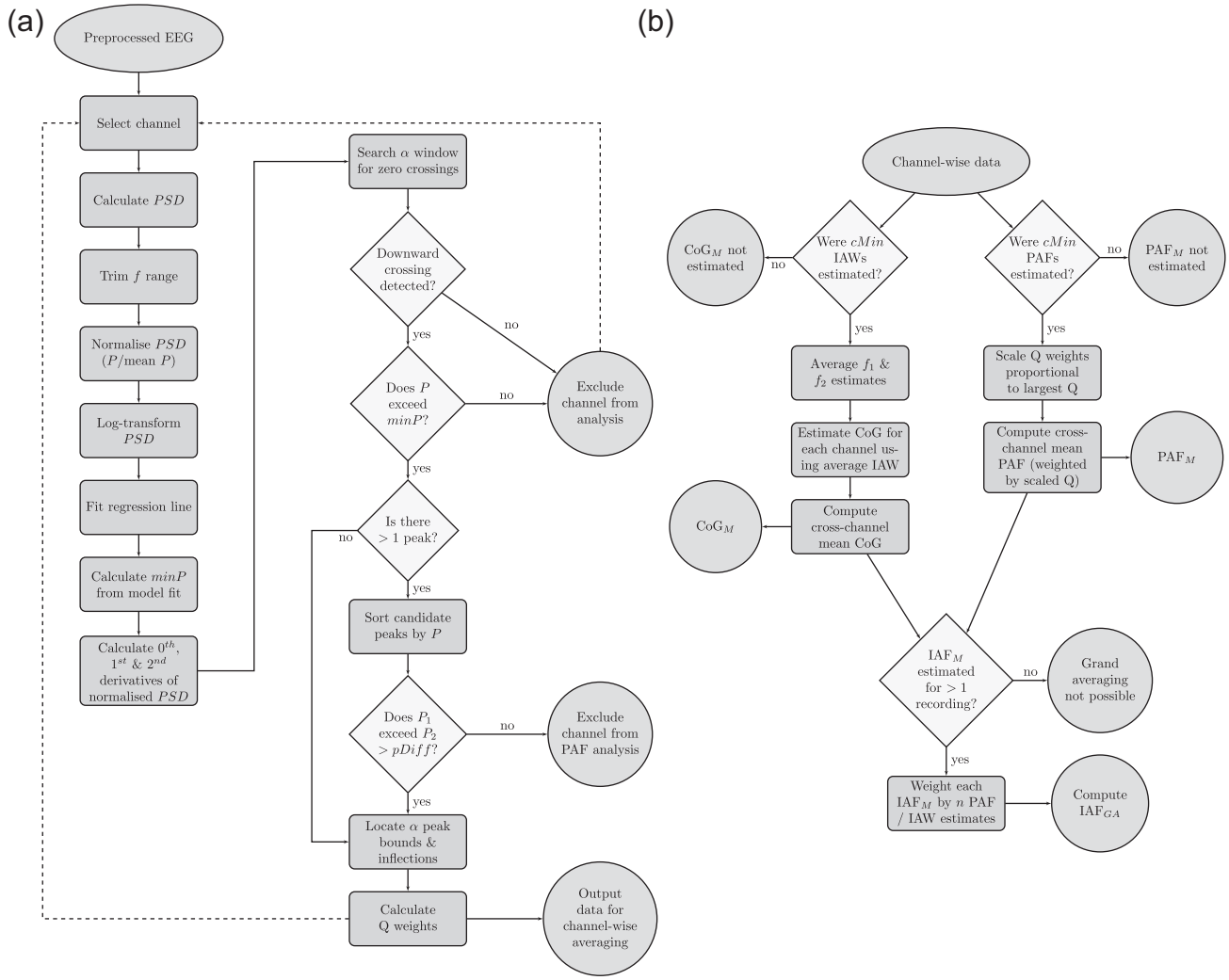

FIGURE 2 Flow diagrams summarizing key steps of the analysis pipeline. (a) Processing of channel data. (b) Cross-channel averaging, assuming a sufficient number of estimates from (a). See main text/Appendix for details. *PSD* = power spectral density; *f range* = frequency bins included in analysis; *P* = power estimate; *minP* = minimum power necessary to qualify as a candidate peak; *pDiff* = minimum power difference necessary to qualify as a PAF estimate; *Q weights* = quantification of relative peak quality (scaled Q value); *cMin* = minimum number of channel estimates required for cross-channel averaging; *IAW* = individualized alpha-band window; f_1 and f_2 = lower and upper bounds of IAW; PAF_M = mean PAF estimate; CoG_M = mean CoG estimate; IAF_M = PAF_M or CoG_M; IAF_{GA} = grand-averaged PAF/CoG estimate

scaled in proportion to the peak with the highest *Q* value, and the (weighted) cross-channel average computed (hence, channels with the strongest evidence of PAF detection contribute more information to the mean estimate of the PAF). We consider this strategy (which only influences results when channel estimates fail to converge) an acceptable trade-off between loss of information (incurred by higher rates of channel exclusion) versus loss of precision (incurred by treating all estimates as equally indicative of the estimand).

2.3 | Empirical EEG data

2.3.1 | Participants

Sixty-three right-handed (Edinburgh Handedness Inventory; Oldfield, 1971), native English-speaking adults (42 female, mean age = 35 years, range = 18–74 years) with normal (or corrected-to-normal) vision and audition, and no history of psychiatric, neurological, or cognitive disorder, participated in the study. All participants provided written, informed consent, and were remunerated for their time. This study was part of a larger research project investigating EEG responses to complex, naturalistic stimuli, and was approved by the University of South Australia Human Research Ethics Committee (Application ID: 0000035576).

2.3.2 | Procedure

Participants were seated in a dimly lit, sound-attenuated room for the duration of the session (2.5–3 hr). Two sets of resting-state EEG recordings were acquired approximately 90 min apart at the beginning and end of an experimental

procedure. This experiment involved watching approximately 70 min of prerecorded television programming, followed by an old/new cued recall task. As per our standard laboratory protocol, both sets of resting-state recordings comprised approximately 2 min of eyes-open EEG followed by 2 min of eyes-closed EEG. Participants were instructed to sit still, relax, and avoid excessive eye movements during this time. Note that only data from the eyes-closed component of the resting-state recordings are reported here (see online supporting information for equivalent analysis of eyes-open data). We favor eyes-closed resting-state data on the basis that it demonstrates (a) greater interindividual variability in alpha power (Chen, Feng, Zhao, Yin, & Wang, 2008), and (b) higher within-session reliability and test-retest stability of IAF estimates (Grandy, Werkle-Bergner, Chicherio, Schniedek et al., 2013) than eyes-open data. Eyes-closed recordings may also be advantageous in reducing ocular artifact.

2.3.3 | EEG acquisition and preprocessing

EEG was recorded continuously from 64 cap-mounted Ag/AgCl electrodes via Scan 4.5 software for the SynAmpsRT amplifier (Compumedics Neuroscan, Charlotte, NC). The online recording was digitized at a rate of 1000 Hz, bandpass filtered (pass-band: 0.05–200 Hz), and referenced to the vertex electrode (AFz served as the ground electrode). Eye movements were recorded from bipolar channels above and below the left eye and on the outer canthi of both eyes. Electrode impedances were maintained below 12.5 kΩ.

EEG data acquired from eyes-closed resting-state recordings were preprocessed in MATLAB 2015a (v8.5.0.197613). All EEG channels were imported into MATLAB via EEGLAB, v13.6.5b (Delorme & Makeig, 2004) and rereferenced to linked mastoids. Each data set was then trimmed to retain only the electrooculogram (EOG) and the nine centroposterior electrodes constituting the region of interest for this analysis: Pz, P1/2, POz, PO3/4, Oz, O1/2. These channels were subjected to zero-phase, finite impulse response high-pass (pass-band: 1 Hz, −6 dB cutoff: 0.5 Hz) and low-pass (pass-band: 40 Hz, −6 dB cutoff: 45 Hz), Hamming-windowed sinc filters (implemented via *pop_eegfiltnew.m* from the *firfilt* v1.6.1 EEGLAB plugin). Automated artifact detection routines were then applied to identify regions of channel data (segmented into 2-s epochs) that contained excessive deviations in the frequency domain (frequency range: 15–40 Hz, spectral threshold: 10 dB). Channels that exhibited an improbable signal distribution (kurtosis z score > 5) were excluded from analysis. EOG channels were removed following artifact rejection, and remaining channels were downsampled to 250 Hz in preparation for spectral analysis. Data sets exceeding 120 s were trimmed to this duration in order to reduce variability in the quantity of data analyzed per participant.

2.3.4 | IAF analysis parameters

Initial parameters for the IAF analysis were determined on the basis of preliminary testing on an independent data set (collected as part of a separate EEG protocol). We implemented *pwelch.m* with a 1,024-sample Hamming window (i.e., four times the sampling rate raised to the next power of 2; window overlap = 50%), yielding a frequency resolution of ∼0.24 Hz. SGF and peak detection parameters were defined as follows: $F_w = 11$ (corresponding to a frequency span of ∼2.69 Hz); $k = 5$; $W_\alpha = [7, 13\ \text{Hz}]$; $pDiff = .20$ (meaning that the largest peak detected within W_α had to be at least 20% higher than any other peak to qualify as the PAF estimate); $cMin = 3$. *minP* was automatically determined for each channel spectrum according to its distributional characteristics.

2.4 | Simulated EEG data

2.4.1 | Single component simulations

As an initial proof of concept, we analyzed the performance of the SGF routine in extracting target alpha frequency components embedded within noisy time series. These composite signals were created by combining a sine wave oscillating at target frequency $F\alpha$ with a 2-min "pink noise" signal (i.e., a randomly sampled signal with a frequency distribution scaled in accordance with the $1/f$ inverse power law). SNR was manipulated by varying the length of the target signal embedded in the composite time series (e.g., for SNR = 0.50, the first half of the signal would comprise the convolution of the alpha and noise signals, whereas the second half would comprise only the noise signal).

We examined PAF estimation at SNR = 0.05, 0.10, 0.15, 0.20, 0.25, 0.30, 0.40, and 0.50, generating 1,000 simulated signals for each SNR level. In addition, we ran a null simulation (SNR = 0) with signals comprised of randomly sampled pink noise only. These SNR levels were arbitrarily selected to explore estimator performance characteristics across a reasonably fine-grained range of relative signal strengths. The target frequency was randomly sampled (with replacement) from a vector ranging from 7.5 to 12.5 in iterations of 0.1. We compared the SGF routine's capacity to extract these target peaks with that of a simple peak detection routine designed to locate the local maximum (LM) within W_α. To avoid spurious estimates from suprema at the lower bound of W_α, this routine evaluated whether the LM exceeded the power estimates of adjacent frequency bins (thus making it functionally equivalent to the first-derivative test). This approach to peak detection—which we consider more robust

than simply relying on the LM alone—was recently reported by Hülsdünker, Mierau, and Strüder (2016) and Milton and Pleydell-Pearce (2017).

Since we are unaware of any automated procedure for estimating the resting-state alpha CoG on the basis of individualized frequency bounds, we were unable to compare our implementation of this estimator to any previously reported standard. All CoG results are therefore reported alongside those of the PAF estimators.

2.4.2 | Mixture and multichannel simulations

Next, we investigated the performance of the SGF routine under more ecologically valid spectral conditions. This involved creating alpha signals that comprised a set of neighboring frequency components from different channels. This configuration was designed to emulate empirical evidence that alpha peaks detected at surface sensors are the product of a distributed network of alpha generators, each oscillating at different frequencies (Barzegaran et al., 2017; Haegens et al., 2014; van der Meij et al., 2016). We did this by sampling an actual/measured alpha frequency per channel from a truncated Gaussian distribution centered at the randomly sampled target $F\alpha$ (selected as for the single component simulation) for each simulated (sub)component (targets chosen uniformly from the standard alpha band, as above). The tails of the Gaussian were truncated ± 2.5 Hz from its mean/target frequency. Alpha signals were thus constructed by creating a weighted average of frequencies within this distribution; in other words, a Gaussian blur was applied to the frequency-domain signal in order to generate a mixture of alpha waves in the time domain.

The area of the Gaussian distribution used to sample the mixed alpha component frequencies was systematically varied by manipulating its α value (i.e., the reciprocal of the standard deviation). Higher α values correspond to narrower distributions, thus rendering composite signals with relatively higher concentrations of frequencies proximal to Fα. We stratified our simulations into three α levels: 1.0, 2.5, and 4.0.

Constructed alpha signals were again combined with pink noise signals at a specified SNR. For these simulations, however, each composite alpha signal was replicated nine times and combined with an independently sampled pink noise signal. This yielded a data set of nine synthetic "channels," each comprising identical alpha signals embedded within stochastically varying background noise. This enabled us to examine how our algorithm's channel exclusion and averaging procedures performed under varying levels of SNR and peak dispersal.

As per the preliminary analysis, we compared the accuracy of SGF-generated PAF estimates against those produced by the LM procedure. For the latter, the optimization function was applied to the mean PSD calculated for each set of simulated channel data. The simulation of broader alpha-band components also afforded the opportunity to assess the performance of our SGF-based CoG estimator.

Finally, we repeated the multichannel simulations using a set of alpha signals sampled via a bimodal Gaussian window. This analysis was designed to replicate troublesome empirical cases in which IAF calculation is complicated by the presence of a split peak—either through poor resolution of a single underlying component, or where dominant activity across multiple alpha generators results in the detection of distinct component peaks at the scalp. This analysis likewise investigated the effect of modulating the composition of the alpha signal, and the SNR of the combined time series, on IAF estimation. As the bimodal sampling window introduced the possibility of more extreme peaks (since peaks necessarily fell either side of the window center), the span of W_α was extended to [6, 14 Hz]. This exception aside, all simulation analyses were implemented using the exact same set of parameters as those described in Section 2.3.4 IAF Analysis Parameters.

3 | RESULTS

3.1 | Empirical EEG data

3.1.1 | Global performance of the SGF routine

Postexperiment resting-state recordings were missing for three participants. A total of 11 channels (all from separate recordings) were excluded on the basis of excessive kurtosis. This left a total 1,096 PSDs to estimate across the sample (pre = 561, post = 535). Of these, a total of 944 PAF (pre = 480, post = 464) and 1,003 CoG (pre = 507, post = 496) estimates were extracted. As Figure 3 indicates, the estimation routine extracted a high proportion of PAF and CoG estimates across most individuals. Two participants failed to surpass the *cMin* threshold for both recordings and were therefore excluded from the PAF analysis. Visual inspection of channel spectra confirmed the absence of any consistent alpha peak. The CoG was, however, estimated for one of these individuals.

3.1.2 | Statistical properties of IAF estimates

Mean IAF estimates were centered about 10 Hz, with the majority falling in the range of 9 to 11 Hz. Both estimators were similarly distributed in both sets of recordings (see Figure 4a). Intraclass correlation coefficients ($ICC_{3,k}$: $PAF_M = .96$; $CoG_M = .98$) indicated that variance in PAF_M and CoG_M estimates was predominantly attributable to inter-individual differences across the sample, rather than intra-individual differences between recordings (see Figure 4b). These data are therefore in accord with previous reports of

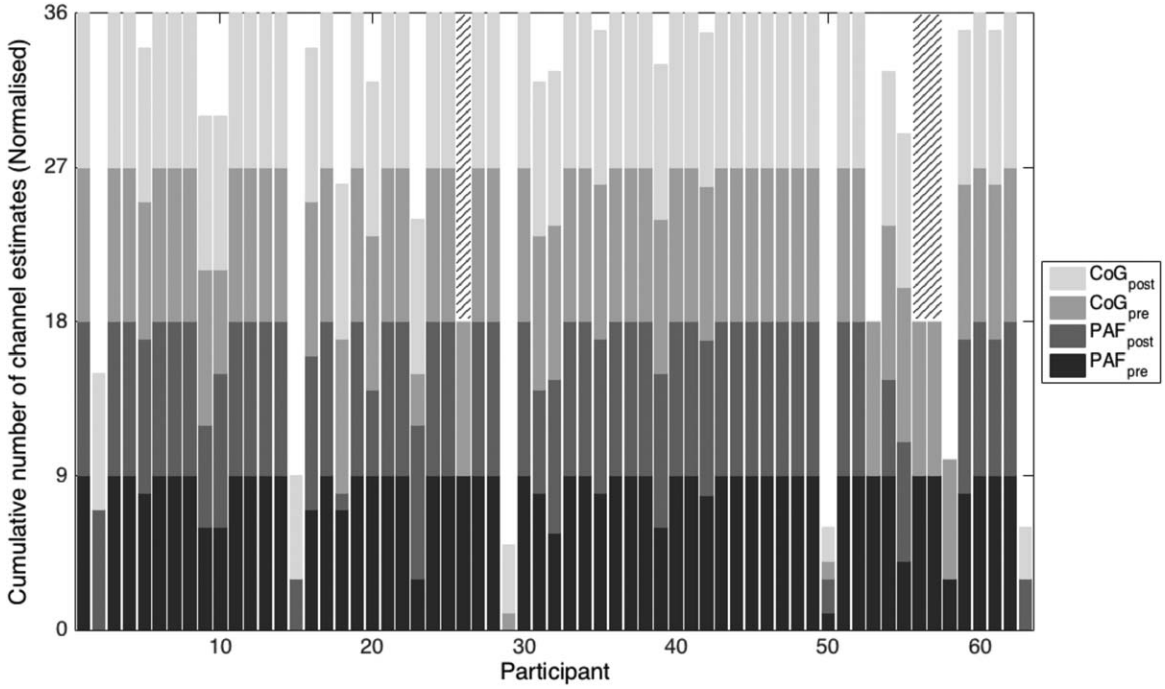

FIGURE 3 Stacked bar chart displaying number of channels from which PAF (lower) and CoG (upper) estimates were derived across participants. Estimates are further divided according to EEG recording (pre/post). Totals normalized to account for excluded channels. Postexperiment data were missing for three participants (indicated by hatching)

the IAF's high temporal stability (at least within the same recording session) and interindividual variability (at least in the context of eyes-closed resting-state EEG).

Kernel density estimation of grand-averaged alpha peak and gravity estimates (PAF_{GA} and CoG_{GA}, respectively) suggested that the probability density function underlying both estimators was well characterized by a Gaussian distribution, although CoG_{GA} was rather more heavy tailed. Despite this difference, PAF_{GA} and CoG_{GA} produced remarkably consistent results ($ICC_{3,k} = .97$; $R^2 = .90$). This finding, which extends that reported in a smaller sample by Jann, Koenig, Dierks, Boesch, and Federspiel (2010), lends weight to the claim that these two estimators tap into the same fundamental oscillatory process(es).

As a final point of comparison with previous findings, we examined the relation between age and IAF (Figure 4b).

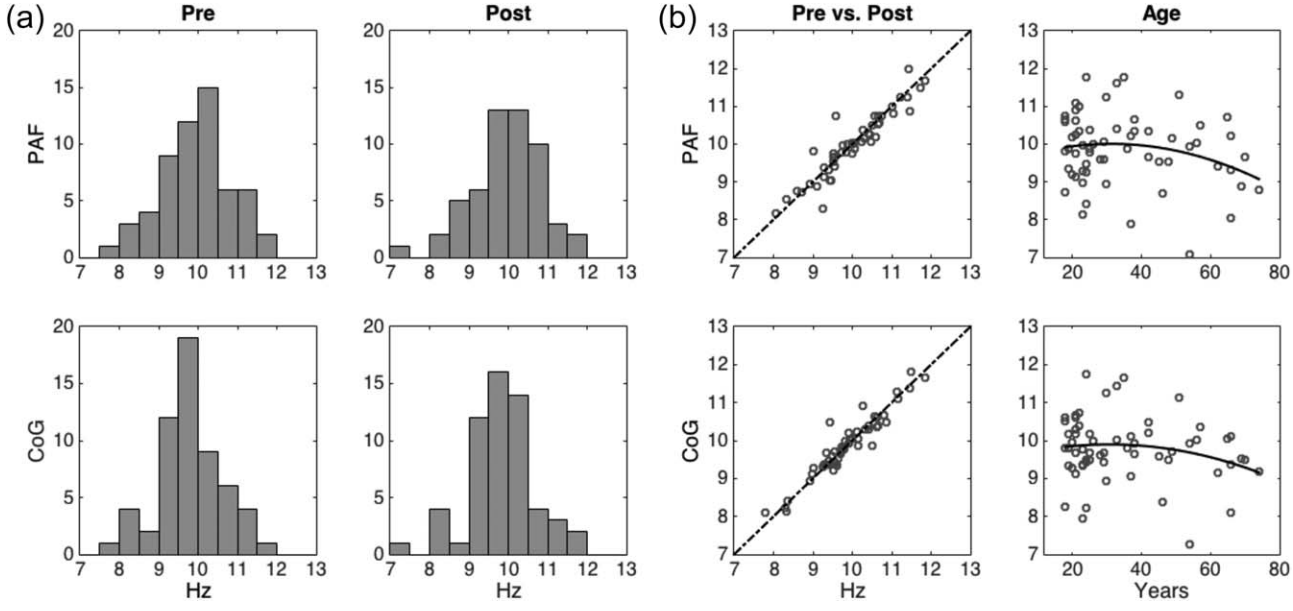

FIGURE 4 Statistical properties of PAF and CoG estimates. (a) Histograms displaying distribution of mean PAF and CoG estimates across pre-/post-experiment recordings. (b) Scatter plots showing correlations between pre-/postexperiment IAF estimates (left), and grand-averaged IAF estimates and age (right). Broken line indicates perfect positive correlation; solid curve indicates 2nd-degree polynomial fit

TABLE 1 Summary statistics characterizing PAF estimation as a function of estimation method and SNR

SNR	0.05	0.10	0.15	0.20	0.25	0.30	0.40	0.50
n PAF								
PAF_{LM}	985	1,000	1,000	1,000	1,000	1,000	1,000	1,000
PAF_{SG}	659	955	997	1,000	1,000	1,000	1,000	1,000
RMSE								
PAF_{LM}	1.06	0.22	0.10	0.08	0.07	0.07	0.07	0.07
PAF_{SG}	0.09	0.09	0.08	0.07	0.07	0.07	0.07	0.07
maxDiff								
PAF_{LM}	5.42	4.83	0.70	0.50	0.50	0.23	0.22	0.14
PAF_{SG}	0.62	0.75	0.75	0.31	0.26	0.18	0.13	0.13
binShift								
PAF_{LM}	224	70	29	8	4	0	0	0
PAF_{SG}	7	14	3	2	1	0	0	0

Note. PAF_{LM} = PAF estimated via the local maximum detection method; PAF_{SG} = PAF estimated via the Savitzky-Golay smoothing method; *n PAF* = total number of PAF estimates extracted from 1,000 simulated time series; *RMSE* = root mean squared error; *maxDiff* = maximum absolute difference (Hz) between estimated and target frequency; *binShift* = number of estimates that diverged from their target frequency by > 0.24 Hz.

Both estimators showed a similar trend toward reduced IAF as age increases beyond the fourth decade. However, this association accounted for a rather small proportion of the variance ($R^2 = .05$ and .04 for PAF_{GA} and CoG_{GA}, respectively). This is consistent with previously reported findings from much larger data sets (e.g., Chiang et al., 2011).

3.2 | Simulated EEG data

3.2.1 | PAF estimator performance as a function of SNR

Preliminary analysis of synthetic EEG data focused on the number of PAF estimates extracted at each SNR level, and how well these estimates approximated the ground truth stipulated by the frequency of the alpha signal embedded in the synthetic time series. In the null simulation, the SGF technique correctly rejected all 1,000 pink noise signals. Following exclusion of 134 peak estimates that failed the suprema check, the LM routine erroneously returned 866 peak estimates on account of spurious fluctuations in the pink noise distribution. For a summary of the results from all other SNR levels, see Table 1.

The SGF technique failed to extract PAF estimates for approximately one third of simulations at SNR = 0.05; however, the proportion of estimated alpha peaks rapidly approached ceiling as SNR increased beyond 0.10. Average error (*RMSE*) was generally low for all levels of SNR, suggesting that alpha peaks were consistently estimated with a high degree of accuracy when detected by the SGF analysis routine. One per cent of PAF estimates in the SNR < 0.15 conditions deviated from their target frequencies by > 0.24 Hz (the approximate frequency resolution of the analysis). Given the general absence of such *binShift* deviations in the higher SNR conditions, and the relatively low magnitude of discrepancies when they did occur, it seems that the SGF technique exhibited near-optimal performance at SNR ≥ 0.30.

The LM routine returned PAF estimates for all simulated spectra; however, 15 estimates in the SNR = 0.05 condition were discarded as lower bound suprema. Even with these estimates removed, LM detection was associated with a 12-fold increase in average estimate error in the SNR = 0.05 condition as compared to the SGF method. Of the 224 estimates that were shifted by more than one frequency bin from their corresponding target frequency, 42 deviated by 1 to 2.5 Hz, while a further 56 deviated by >2.5 Hz. All of these extreme errors constituted underestimates of the target component. The LM procedure was also markedly less accurate in the SNR = 0.10 condition, where it registered more than double the *RMSE* of SGF-resolved peaks. Average LM estimation error converged with that of the SGF technique in higher SNR conditions, although the magnitude of worst errors (*maxDiff*) remained elevated relative to SGF-generated PAF estimates.

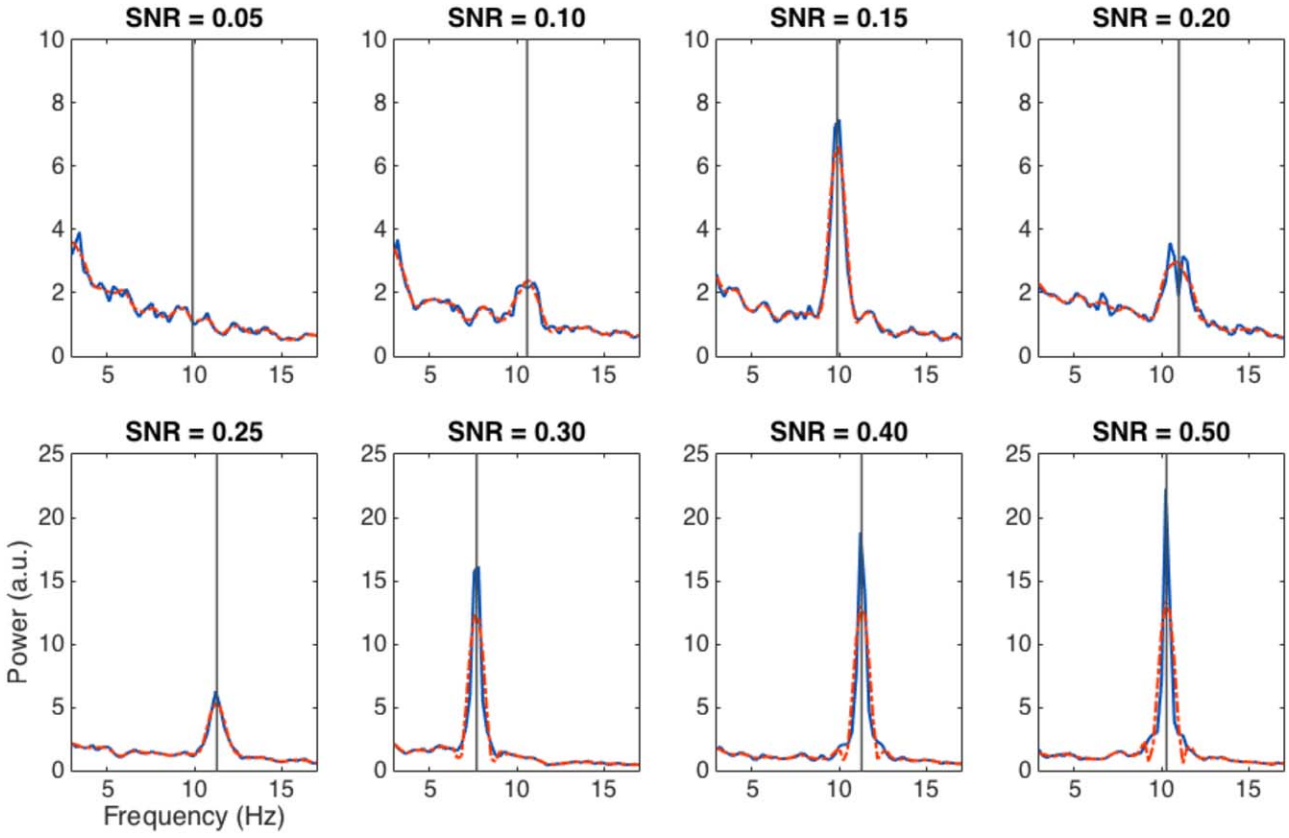

FIGURE 5 Channel spectra randomly sampled from each SNR condition. Solid blue functions represent PSD estimates generated by *pwelch.m*. Broken red functions indicate the effect of smoothing these estimates with the Savitzky-Golay filter. Target alpha component frequency $F\alpha$ indicated by vertical line. *a.u.* = arbitrary unit

To give a flavor of how smoothing may have influenced the PSD estimates generated by *pwelch.m* at each SNR level, a selection of simulated PSD functions is illustrated in Figure 5. Both techniques return identical PAF estimates at the highest SNR levels. The SGF also tends to attenuate peak height, as would be expected of a smoothing procedure. The SNR = 0.30 panel reveals one instance where the application of the smoothing procedure to a somewhat blunted component structure results in the erroneous ascription of PAF to a neighboring frequency bin. The advantages of the SGF technique are thrown into relief, however, by two scenarios in which the LM estimator errs. In the SNR = 0.05 panel, the LM routine identifies a spurious fluctuation at 7.57 Hz as the PAF ($F\alpha = 9.9$ Hz). Here, the LM technique is disadvantaged by its inability to evaluate whether the detected LM constitutes a substantial deviation from background noise. In contrast, the SGF routine finds insufficient evidence of peak activity within the alpha search window, and thus does not return any estimate of PAF. The second scenario arises when the target component is suboptimally resolved by *pwelch.m*, resulting in either a broad structure featuring two maxima (SNR = 0.10) or a more clearly defined split peak (SNR = 0.20). In both cases, smoothing helps to recover the shape of the peak component underlying the spectral data, thus culminating in more veridical PAF estimates than those derived via the LM method.

In sum, this preliminary analysis provides compelling evidence that the SGF method generally furnishes accurate estimates of the PAF when a singular alpha component is present within the PSD. Such accuracy is maintained even at relatively low SNR levels, although the extraction of low-powered peaks amid background noise becomes more challenging when SNR drops below 0.15. The more conservative nature of the SGF method (as compared to LM detection) in the context of low SNR may, however, be advantageous in protecting against inaccurate PAF estimates issuing from spurious background fluctuations.

3.2.2 | Multichannel data set simulations

Given that the PAF estimators approached ceiling performance at moderate levels of SNR in the previous analysis, we limited multichannel simulations to a low (0.15) and a moderate (0.40) SNR condition. A total of 100 data sets, each comprising nine synthetic EEG channels, were simulated for each level of alpha component dispersal in

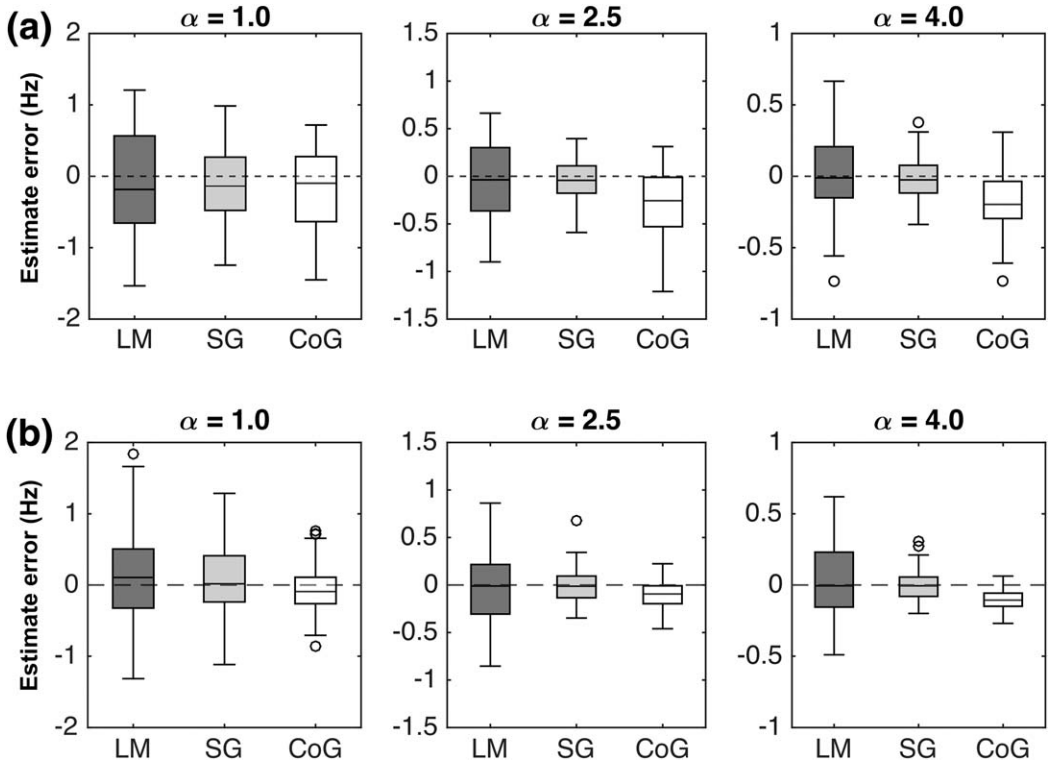

FIGURE 6 Box plots summarizing spread of estimator error across simulation conditions. Center marks indicate median error, edges indicate interquartile range (IQR), whiskers indicate approximately 1.5 × IQR. Zero estimate error (broken horizontal line) corresponds to extraction of the target alpha peak frequency. Negative error indicates underestimation of the target frequency, positive error indicates overestimation. SNR set to 0.15 in (a), 0.40 in (b). Dispersal of the target alpha component broadest in the left column (α = 1.0) and narrowest in the right (α = 4.0). *LM* and *SG* = PAF estimated via the local maximum and Savitzky-Golay routines, respectively. *CoG* = CoG estimated via the Savitzky-Golay routine. *Y* axis scaling varied across α levels to aid visualization

both SNR conditions (yielding a total of 5,400 PSD estimates). The results of this analysis are summarized in Figure 6 and Table 2.

Across all Distribution × SNR conditions, the SGF routine failed to generate average PAF estimates for 11 data sets. Eight of these instances occurred in the low SNR condition (7 $\alpha = 1.0$; 1 $\alpha = 2.5$), while the remainder occurred when attempting to recover broad component structures ($\alpha = 1.0$) in the moderate SNR condition. By contrast, both the LM and the CoG estimators rendered estimates for all 600 simulated data sets.

All three estimators demonstrated consistent reductions in error as alpha component dispersal diminished (i.e., as target peaks became narrower). This finding is congruent with the intuition that, irrespective of SNR, recovery of broader component structures poses a greater challenge for automated estimation procedures than the recovery of narrower, sharper peaks. Further, there was some indication of a Distribution × SNR interaction effect, such that error indices for a given α level were more elevated in the low (as compared to the moderate) SNR condition. Although this effect was somewhat marginal (and not entirely consistent) for the PAF estimators, it was more clearly apparent for the CoG estimator. These general trends (i.e., improved estimation accuracy with decreased component dispersal and increased SNR) were mirrored by both the average (median) number of channels that contributed to PAF_{SG} estimation, and the degree of variability (*SD*) in the number of channels retained by the SGF procedure for IAF estimation in each set of simulations. This is to say that a higher proportion of channels rendered PAF estimates as SNR increased and peak dispersal decreased, while volatility in the number of channels selected for mean PAF/IAW estimation correspondingly declined.

As per the single component analysis, PAF estimates from low SNR simulations were more accurate on average when estimated with the SGF procedure. Unlike the prior analysis, however, the *RMSE* of PAF_{LM} failed to converge with that of PAF_{SG} in the moderate SNR condition (indeed, *RMSE* of the former was more than double that of the latter for both intermediate and narrow peak estimates). The magnitude of worst estimate errors (*maxDiff*) was likewise consistently elevated for PAF_{LM} as compared to PAF_{SG}-generated estimates. Perhaps most notably, PAF_{LM} produced considerably more estimate errors in excess of ± 0.5 Hz than PAF_{SG} (27% vs. 11%). This contrast was most stark at $\alpha \geq 2.5$, where the error rate associated with PAF_{LM} was 14% (compared to < 1% for PAF_{SG}).

TABLE 2 Estimator performance as a function of SNR and alpha component distribution

SNR		0.15			0.40	
α	1.0	2.5	4.0	1.0	2.5	4.0
RMSE						
PAF_{LM}	0.72	0.38	0.30	0.63	0.38	0.26
PAF_{SG}	0.47	0.21	0.15	0.48	0.17	0.10
CoG	0.57	0.45	0.27	0.34	0.16	0.12
maxDiff						
PAF_{LM}	1.53	0.90	0.73	1.84	0.86	0.62
PAF_{SG}	1.24	0.59	0.38	1.29	0.68	0.31
CoG	1.45	1.21	0.73	0.86	0.46	0.27
% Dev						
PAF_{LM}	63	17	14	42	22	3
PAF_{SG}	30	2	0	33	1	0
CoG	42	30	7	18	0	0
n chans						
PAF_{SG}	5 (1.81)	6 (1.53)	8 (1.23)	5 (1.52)	7 (1.27)	9 (0.70)
CoG	9 (0.79)	9 (0.36)	9 (0.10)	9 (0)	9 (0)	9 (0)

Note. α = 1.0 corresponds to a broad peak, α = 4.0 a narrow peak. PAF_{LM} = local maximum PAF estimator; PAF_{SG} = Savitzky-Golay filter (SGF) PAF estimator; *CoG* = SGF CoG estimator; *RMSE* = root mean squared error; *maxDiff* = maximum absolute difference (Hz) between estimated and target frequency; *% Dev* = percentage of estimates that diverged from the target frequency by > 0.5 Hz; *n chans* = median (*SD*) number of channels furnishing PAF/IAW estimates per simulated data set.

Comparison of SGF-generated estimates of PAF and CoG discloses an interesting interaction between estimator performance and SNR. While the PAF estimator resulted in diminished *RMSE*s, lower maximal deviations, and fewer estimation errors ± 0.5 Hz in the low SNR simulations, this pattern was inverted (with the exception of one *RMSE* value) in the moderate SNR condition. This latter result provides encouraging evidence in favor of our method's capacity to accurately localize the beginning and end of the IAW (at least when the embedded alpha signal is not too weak). Interestingly, even though the CoG performed less consistently when SNR was low, it still tended to be more reliable than the PAF_{LM} estimator. For instance, the CoG method resulted in a 16% reduction in substantial estimate errors compared to the LM method. While CoG may therefore be more susceptible to bias than its PAF_{SG} counterpart when channel spectra contain relatively high degrees of background noise, it may still offer tangible advantages over LM-based peak detection strategies.

3.2.3 | Split-peak simulations

Finally, we repeated the multichannel data set simulations with composite signals constructed using a bimodal sampling window. This window comprised two overlapping Gaussians (α = 2.5), the right-most of which was scaled equal to, 0.25, or 0.50 times larger than its counterpart. The frequency offset between the two Gaussian peaks was equivalent to 1.6 Hz. The results of this analysis are summarized in Figure 7 and Table 3.

PAF_{SG} failed to find evidence of a distinct peak in 11% of low SNR data sets (equal = 14, +0.25 = 7, +0.50 = 11), and 2% of moderate SNR data sets (equal = 3, +0.25 = 4, +0.50 = 0). Median number of channel PAF estimates was also reduced as compared to the corresponding SNR conditions in the single-peak, multichannel simulations. PAF_{LM} and CoG returned estimates for all 600 simulated data sets.

Across all conditions, PAF_{LM} returned more variable and extreme results than PAF_{SG}, although interpretation of this observation is complicated by the presence of a (somewhat) dominant peak in the +0.25 and +0.50 conditions. As SNR and peak differences increase, PAF_{LM} shows stronger migration toward the higher frequency peak than either of the SGF estimators, although note that it is still more prone to erroneously ascribing the PAF to the secondary (lower frequency) peak (see Figure 7). On the other hand, PAF_{SG} is less liable to spurious fluctuations in the PSD, tending instead to curb PAF estimation toward the center mass of the double component. This might suggest that marginal local maxima are absorbed within the recapitulation of a broader peak structure as a consequence of spectral smoothing. As SNR and peak inequality increase, PAF_{SG} estimates cluster in closer proximity to the dominant peak. This explains why *RMSE* increases relative to the center frequency: as SNR improves and the split peak becomes more asymmetrical (and hence, one peak more dominant over its competitor), more evidence accrues in favor of an underlying PAF.

The CoG estimator demonstrates an intermediate level of variability compared to the PAF estimators under low SNR conditions, but is markedly less variable under moderate SNR conditions. The box plots in Figure 7 also indicate that the CoG estimator performed similarly across the different degrees of peak inequality within each SNR level. Irrespective of peak scaling, CoG estimates were substantially more precise when SNR = 0.40. Indeed, compared to the other two estimators, CoG is both remarkably stable and closely centered around the center frequency of the window function (which coincides with the true CoG in the context of equal peaks, and closely approximates it in the unequal conditions). As such, this finding provides compelling evidence that our implementation of the CoG estimator renders an accurate summary of the underlying alpha component distribution.

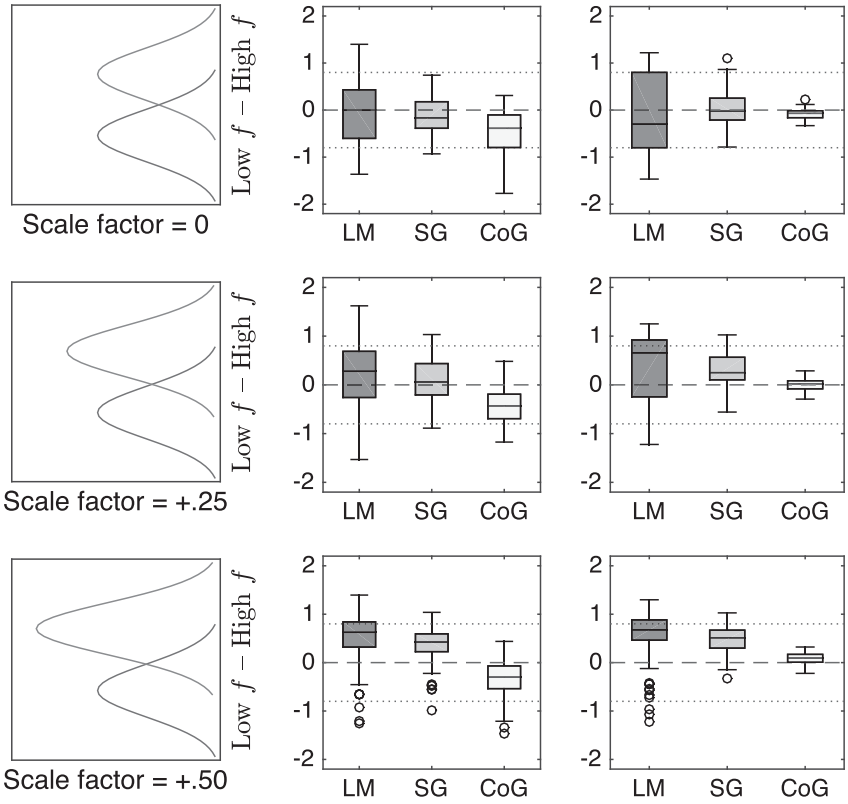

FIGURE 7 Box plots summarizing spread of estimate deviation from the center frequency of the sampling window. Center marks indicate median deviation, edges indicate interquartile range (IQR), whiskers indicate approximately 1.5 × IQR. Zero deviation (broken horizontal line) corresponds to estimating the midpoint between the two components. Peak locations indicated by dotted horizontal lines. Left: Schematic of the sampling window used to construct composite alpha signals simulated in corresponding row. Discrepancy between simulated peaks (higher relative to lower frequency bins) ranges from 0 (top to +0.50 bottom). *LM* and *SG* = local maximum and Savitzky-Golay PAF estimates, respectively. *CoG* = Savitzky-Golay CoG estimates

4 | DISCUSSION

We have proposed a novel method for estimating the two most prevalent indices of IAF in the literature. This method pairs a common approach to the automated detection of local maxima (i.e., searching for first-derivative zero crossings) with a well-established method of resolving spectral peaks (i.e., Savitzky-Golay filtering) to derive an estimate of PAF. It also extends the logic of the first-derivative test to estimate the bounds of the alpha peak component, thus enabling calculation of the (individualized) alpha-band CoG. Like other automated curve-fitting algorithms reported in the literature (e.g., Chiang et al., 2008; Lodder & van Putten, 2011), this method addresses key limitations of visual PSD analysis (e.g., proneness to subjective bias, inefficiency, poor replicability), while improving upon alternative automated approaches that may be prone to various artifacts (e.g., failure to differentiate a single dominant peak from competing spectral peaks or spurious fluctuations, reliance on alpha-band reactivity). Unlike these algorithms, however, our method is openly accessible and easy to integrate within existing MATLAB and Python-based analysis pipelines.

Our results demonstrate that the SGF technique can extract a high proportion of IAF estimates from an empirical data set, and that the samplewide properties of these estimates (intraindividual stability, interindividual variance, age-related trends, etc.) are consonant with prior reports in the literature. Furthermore, application of the technique to simulated data sets verified its ability to render accurate estimates of peak location, even under highly degraded SNR conditions. When extended to more complex simulations, the SGF technique was shown to recover target values with greater precision than an alternative peak detection method. We begin by considering the key findings of our analyses, before reflecting on present limitations and potential directions for future research.

4.1 | Estimating IAFs from an empirical EEG data set

Savitzky-Golay filtering of *pwelch.m*-generated PSD functions resulted in the extraction of a rather impressive number of IAF estimates from a moderate-sized data set. This suggests our technique offers substantive benefits in terms of data retention in comparison to subjective analysis, which can result in high rates of attrition if dominant peaks cannot be confidently distinguished from background noise (e.g., Bornkessel-Schlesewsky et al., 2015). We note also that our

TABLE 3 Estimator performance as a function of SNR and relative weighting of bimodal peaks

SNR		0.15			0.40	
PeakDiff	0	+0.25	+0.50	0	+0.25	+0.50
RMSE						
PAF_{LM}	0.69	0.69	0.75	0.84	0.79	0.76
PAF_{SG}	0.40	0.44	0.51	0.38	0.45	0.55
CoG	0.62	0.56	0.51	0.14	0.12	0.15
maxDiff						
PAF_{LM}	1.40	1.62	1.40	1.47	1.25	1.30
PAF_{SG}	0.93	1.03	1.04	1.10	1.03	1.03
CoG	1.77	1.17	1.47	0.33	0.29	0.32
n chans						
PAF_{SG}	4 (1.52)	5 (1.49)	5 (1.68)	5 (1.36)	6 (1.64)	6 (1.31)
CoG	9 (0.46)	9 (0.48)	9 (0.51)	9 (0)	9 (0)	9 (0)

Note. Right-most Gaussian function was either 0, 0.25, or 0.50 times larger than the left (*PeakDiff*). PAF_{LM} = local maximum PAF estimator; PAF_{SG} = Savitzky-Golay filter (SGF) PAF estimator; *CoG* = SGF CoG estimator; *RMSE* = root mean squared error (relative to center frequency of sampled components); *maxDiff* = maximum absolute difference between estimates and center frequency of sampled components; *n chans* = median (*SD*) number of channels furnishing PAF/IAW estimates per data set.

SGF method furnished a higher proportion of PAF estimates than that produced by the Gaussian curve-fitting procedure implemented by Haegens and colleagues (2014). It may be the case that our nonparametric approach, which attempts to smooth the PSD rather than fit a specified function to it, retains more data by virtue of its capacity to accommodate a broader range of alpha-band distributions.

By the same token, it is reassuring that neither of the two cases in which the technique failed to extract PAF estimates demonstrated compelling evidence of any concerted alpha peak activity on visual inspection of their respective PSD plots. It is also worth pointing out that the diverse age range of participants within this study is likely to have posed a nontrivial challenge to any automated alpha-band quantification routine, given the typically reported changes in both spectral power and distribution associated with older adulthood (e.g., Dustman, Shearer, & Emmerson, 1999). That our technique was able to extract estimates from the vast majority of sampled individuals, and that it did so using a fixed set of parameters defined a priori on the basis of preliminary testing in an independent data set, speaks to its capacity to derive resting-state IAF estimates across a broad spectrum of the healthy population.

Comparison of grand-averaged PAF and CoG estimates revealed a high degree of intercorrelation, despite certain differences in their distribution. Although this might prompt concerns of redundancy, we interpret this finding positively: the CoG seems to tap into a similar underlying neural process (or set of processes) as the PAF. Although not necessary in the present analysis on account of the high proportion of PAFs that were extracted across participants, this finding suggests that the CoG estimator might warrant deployment as an alternative marker of IAF in cases where the PAF cannot be obtained. In any case, given the dearth of research directly comparing these two measures (most IAF-related research involves some variant of the PAF, perhaps on account of the additional complexities involved in calculating the CoG), we suggest it would be informative if investigators adopted the policy of reporting both indices in parallel. Should it be the case that PAF and CoG track one another almost identically, then only one of these measures need be selected for the remaining analysis (see, e.g., Jann et al., 2010). However, if it turns out that PAF and CoG diverge under certain circumstances, delineating such cases might help improve our understanding of the IAF (and alpha-band dynamics more generally). It is, of course, a notable advantage of our method that it enables investigators to rapidly derive samplewide estimates of PAF and CoG simultaneously, thus furnishing a convenient means of estimator comparison. To the best of our knowledge, no previously reported automated technique provides this functionality.

Although the analysis parameters we implemented in the SGF routine worked well for this data set, we do not insist that these settings ought to be the default standard in all future analyses. Rather, parameters should be thoughtfully defined in accordance with expectations about the general characteristics of alpha-band activity under study-specific conditions. For instance, filter settings (F_w and k) will depend on the anticipated noisiness and dispersal of alpha component activity, while peak detection (*minP* and *pDiff*) and channel averaging (*cMin*) criteria will depend on the amount of available data and the trade-off between liberal and conservative detection thresholds (a problem that is intrinsic to traditional methods of PAF estimation). Some degree of exploratory analysis may therefore be necessary in order to tune analysis parameters to the data at hand. We do not see this as inherently problematic so long as the distinction between exploratory and confirmatory modes of analysis is respected. As with any form of data processing, we urge investigators to be transparent about the rationale motivating their choice of parameter settings, and to apply such settings consistently across the data set prior to inferential statistical analysis.

4.2 | Estimation of simulated IAFs

Our preliminary simulation analyses indicated that the SGF technique approached an optimal level of performance when

2-min synthetic signals consisted of approximately 36 s of alpha-band oscillations (SNR = 0.30). Indeed, the peak detection routine performed reasonably well when signals contained as little as 12 s of alpha-band activity, with fewer than 6% of simulated alpha components going undetected or erroneously estimated by the equivalent of more than one frequency bin (i.e., > 0.24 Hz).

Interestingly, our analysis shows that less sophisticated approaches to peak estimation can result in substantial error at relatively low levels of SNR. It is likely that most of these inaccurate estimates derived from spurious local maxima occurring due to random fluctuations in background spectral activity (indeed, this is the only possible explanation for false positives in the SNR = 0 simulation). The LM method's propensity to underestimate PAF in low SNR conditions supports this interpretation, since the inverse power law (which is not generally taken into account by LM detection methods) increases the probability of spurious local maxima at lower frequencies within the search window. Such artifacts are undesirable not only for the obvious reason that they introduce additional noise into IAF-related analyses, but also because such errors diminish confidence in automated analysis methods more generally (after all, such errors would presumably have been avoided had spectral data been subjected to visual inspection). Indeed, we consider it preferable that an automated peak detection routine should reject spectra showing inconclusive evidence of any concerted alpha-band activity, rather than generate highly deviant estimates of the underlying (albeit weak) signal. Thus, it is a strength of the SGF technique that it applies more stringent criteria in the evaluation of candidate peaks.

In addition to demonstrating that the SGF technique consistently outperforms the LM approach in low-to-moderate SNR conditions, our analysis also confirmed that the application of this smoothing procedure did not cause excessive distortion of PAF estimates. Furthermore, our analysis highlighted that discrete Fourier analysis methods (such as Welch's modified periodogram) might precipitate artifactual split peaks, and that such cases can be ameliorated by means of a smoothing procedure. Consequently, the single component simulation analysis stands as a basic proof of concept that the SGF method is capable of (a) extracting a high proportion of underlying peak frequencies without introducing systematic bias, and (b) improving upon existing techniques of peak resolution and estimation, thus helping to maximize the number of IAF estimates that can be obtained from a given data set. We acknowledge, however, that the estimation of sharply defined, single-frequency alpha components may well be unrepresentative of genuine electrophysiological data in many contexts. While it is encouraging that the SGF technique performed well under these reasonably favorable conditions, it was necessary to demonstrate its capabilities when confronted with more complex, ecologically valid signals.

The multichannel simulation analyses were designed to be more faithful to empirical resting-state EEG data, in as much as each target signal comprised a range of alpha components embedded within a variety of nonidentical (but highly correlated) time series. These simulations also enabled us to examine the performance characteristics of the SGF routine's CoG estimator, which was expected to closely approximate the PAF in the context of Gaussian-distributed alpha components. The critical finding across all simulation conditions was that the SGF technique rendered PAF and CoG estimates that almost always improved upon LM-derived PAF estimates from averaged channel spectra. This finding held irrespective of whether estimator deficits were quantified in terms of the average error across simulated data sets, magnitude of worst (i.e., most deviant) estimate errors, or percentage of estimates in the data set that deviated from the ground truth by more than ± 0.5 Hz (a threshold previously used by Lodder & van Putten, 2011, to evaluate the performance of their peak detection algorithm).

Leaving aside the superiority of the SGF over the LM detection routine, one might still raise the concern that its performance falls somewhat short when applied to broadly dispersed alpha component structures. Indeed, the *RMSE* of the PAF estimator in both SNR conditions of the single-peak analysis approaches the ± 0.5 Hz threshold demarcating substantial estimate deviation, while the CoG exceeds this limit when SNR is low. Correspondingly, low-α multichannel simulations returned a much higher proportion of estimates exceeding the ± 0.5 Hz error threshold (as compared to simulations involving higher α levels), especially in the case of the PAF estimator. It ought to be borne in mind, however, that all simulation analyses were performed using SGF parameters identical to those used in the empirical analysis. This is pertinent because it is likely that the filter frame width (F_w=11) was suboptimally narrow for the purpose of smoothing such broad peak structures. Indeed, post hoc analysis (not reported) revealed that simply doubling the length of the filter frame can halve the number of simulations that failed to produce PAF estimates, as well as reduce substantial estimate deviation by one third under moderate SNR conditions. Corresponding improvements were not realized, however, in the context of low SNR; hence, the recovery of broadly dispersed, relatively weak alpha signals remains technically challenging.

Of the three IAF estimators examined in these simulations, the CoG was most sensitive to manipulation of the SNR. That low SNR simulations should inflict notable performance decrements is hardly surprising, however, given that CoG calculation depends upon the spectral characteristics of the entire (individualized) alpha-band interval across all available channels. Not only does low SNR pose nontrivial difficulties in

defining the bounds of the alpha interval (thus threatening to introduce noise by either including extraneous data from beyond the alpha interval, or excluding portions of the alpha band from analysis), the relative weakness of the alpha signal means that a higher proportion of background noise contributes to CoG calculation. This scenario may be compounded by the fact that the traditional method of computing CoG estimates averages across all available channels, not just those that contributed to calculation of the IAW (although note that the average number of channels selected to infer this bandwidth remained high even in the doubly challenging conditions posed by the low SNR × broad component dispersal combination of the single-peak analysis). It might be the case then that the central tendency-like properties of the CoG, which may have underpinned its strong performance in the moderate SNR simulations (where, of the three estimators, it was the least prone to substantial estimate deviation), render it more vulnerable to error when alpha-band activity is relatively sparse. Consequently, it could be useful to investigate whether the performance of the CoG estimator in relatively noisy conditions can be augmented through the development of more robust methods of calculation.

Taking the results of the single- and split-peak simulations together, it is tempting to conclude that the PAF estimator outperforms its CoG counterpart in the former scenario, while the opposite is true in the latter. Even under relatively favorable spectral conditions, the CoG estimator tended to underestimate the target frequency in the single-peak simulations. Indeed, CoG estimates increasingly deviated from the center frequency of the target component as the latter became narrower, which seems counterintuitive if such peaks ought to be less difficult to resolve and parameterize. We suggest, however, that this tendency derived from the skewness introduced into the Gaussian-distributed target components when they were combined with the pink noise signal. This observation thus reinforces the point that PAF and CoG estimators summarize different features of the spectral distribution, and that they need not always converge. Analysis of the split-peak simulations suggests, however, that the SGF method may still be somewhat prone to PAF estimate distortion when the underlying *pwelch.m* routine fails to consistently resolve dual subcomponents across channel spectra. This finding suggests a more stringent *cMin* criterion may be advisable to avoid PAF estimates that might in fact reflect a more CoG-like average across channels that, due to random noise fluctuations, resolve only one of two (or more) underlying components. In our view, the fact that the SGF approach to PAF estimation does not fully eliminate the methodological and conceptual challenges posed by split peaks is not so much an intrinsic shortcoming of our technique in particular, but reflects rather a problematic attribute of the PAF in general. These data thus lend weight to the argument that the CoG, insofar as it avoids these difficulties, might be preferable to the PAF.

4.3 | Limitations and future developments

We aimed to design an accessible, fast, automated routine that calculates reliable PAF and CoG estimates from posterior channel EEG data recorded during short periods of relaxed, eyes-closed wakefulness. Although limited in its current scope, we believe that the algorithm could be adapted for application across a broader range of empirical contexts (e.g., quantifying spectral dynamics across various frequency bands during task-related activity; quantifying peak characteristics across different topographical regions). It may prove more challenging, however, to accurately resolve estimates of IAF under conditions that are less conducive to the manifestation of a dominant alpha peak (or indeed, in populations known to manifest spectral characteristics that differ from those of neurotypical adults). Further research would therefore be required to establish the utility of the SGF technique for applications beyond the rather circumscribed conditions examined here.

Notably, any attempt to extend the SGF technique beyond its current scope must acknowledge the simplifying assumption (shared by many conventional approaches to IAF estimation) that alpha activity is meaningfully characterized by a single summary statistic (moreover, one that is biased toward the strongest alpha generator). This approach discounts the possibility that the neuronal sources that contribute to the posterior alpha rhythm possess functionally distinct properties. For instance, Gulbinaite, Ilhan, and VanRullen (2017) recently showed that the modulation of an illusory percept is strongly predicted by prestimulus activity in parietal (but not occipital) alpha components. This finding suggests that IAF-related analysis of individual differences in task performance might benefit from strategies that are sensitive to potential disparities across distinct sources of alpha activity. One promising possibility would be to combine our spectral smoothing approach with a method of sensor-level component decomposition, such as independent component (e.g., Gulbinaite, Ilhan, & VanRullen, 2017; Gulbinaite, van Viegen, Wieling, Cohen, & VanRullen, 2017), parallel factor (e.g., Barzegaran et al., 2017), or phase coupling-based (e.g., van der Meij et al., 2016) analysis.

One aspect of performance that was not investigated in our analysis was whether the accuracy and precision of IAF estimates depend upon the method used to derive underlying PSD estimates. In its present implementation, our algorithm relies upon Welch's method to estimate the PSD that is ultimately subjected to the SGF's smoothing and differentiation operations. It may therefore be worthwhile to investigate whether alternative methods of PSD estimation (e.g., the multitaper method, continuous wavelet transform) can be

exploited in conjunction with the SGF technique in order to further improve IAF estimation.

Another potential opportunity for optimizing the performance of the SGF routine would be to develop a function that automatically adapts the F_w (filter width) and k (polynomial degree) parameters in accordance with the approximate span of the dominant frequency component located within the search window W_α. This could be achieved via an iterative fitting procedure, where the empirical features of the alpha-band component are initially parameterized in order to scale F_w and k. Once these parameters have been determined for the data at hand, smoothing and estimation procedures could proceed as described above. Not only would this process potentially increase the number of IAF estimates that can be accurately obtained from a given data set, it would reduce the number of free parameters that must be defined in order to implement the algorithm.

Finally, it would be desirable to create a package that incorporates the MATLAB implementation of the SGF routine within the EEGLAB graphic user interface. Not only would this help to make the procedure accessible to the broadest possible range of EEGLAB users, it would also provide a convenient platform for integrating visualizations of the spectral analysis that may (for instance) assist in the diagnosis of suboptimal parameter settings. We intend to explore a number of these possibilities in future work.

4.4 | Conclusion

We have developed a free, open-source program for automatically estimating individual alpha frequency in resting-state EEG data. This program has been shown to perform more accurately than a common approach to automated peak detection, and may return a higher proportion of empirical IAF estimates than techniques relying on parametric curve-fitting procedures. Furthermore, this method is not dependent on phasic changes in alpha-band reactivity, which may produce biased IAF estimates. In addition to its obvious advantages in terms of efficiency and replicability, our simulations indicate that this method could help to improve the accuracy and precision of future IAF-related research. This technique may also open up new lines of methodological inquiry, insofar as it facilitates the direct comparison of two prevalent indices of IAF that have, for the most part, been investigated in isolation of one another.

ACKNOWLEDGEMENTS

We thank Jessica Gysin-Webster and Daniel A. Rogers for their assistance with data collection. We would also like to thank the reviewers for their thoughtful criticisms and insights. This work was partially supported by funding from the University of South Australia Ehrenberg-Bass Institute for Marketing Science. This funding supported A. W. C. while he collected and analysed the empirical EEG data set reported in this manuscript. The Institute had no influence on the design, analysis, or interpretation of the reported study.

ORCID

Andrew W. Corcoran http://orcid.org/0000-0002-0449-4883
Phillip M. Alday http://orcid.org/0000-0002-9984-5745
Matthias Schlesewsky http://orcid.org/0000-0003-4131-8077
Ina Bornkessel-Schlesewsky http://orcid.org/0000-0002-3238-6492

REFERENCES

Adrian, E. D., & Matthews, B. H. C. (1934). The Berger rhythm: Potential changes from the occipital lobes in man. *Brain*, *57*, 355–385. https://doi.org/10.1093/brain/57.4.355

Barzegaran, E., Vildavski, V. Y., & Knyazeva, M. G. (2017). Fine structure of posterior alpha rhythm in human EEG: Frequency components, their cortical sources, and temporal behavior. *Scientific Reports*, *7*, 8249. https://doi.org/10.1038/s41598-017-08421-z

Başar, E. (2012). A review of alpha activity in integrative brain function: Fundamental physiology, sensory coding, cognition and pathology. *International Journal of Psychophysiology*, *86*(1), 1–24. https://doi.org/10.1016/j.ijpsycho.2012.07.002

Bazanova, O. M., & Vernon, D. (2014). Interpreting EEG alpha activity. *Neuroscience & Biobehavioral Reviews*, *44*, 94–110. https://doi.org/10.1016/j.neubiorev.2013.05.007

Berger, H. (1929). Über das elektrenkephalogramm des menschen [On the electroencephalogram of man]. *Archiv für Psychiatrie und Nervenkrankheiten*, *87*, 527–570. https://doi.org/10.1007/bf01797193

Bornkessel, I. D., Fiebach, C. J., Friederici, A. D., & Schlesewsky, M. (2004). "Capacity" reconsidered: Interindividual differences in language comprehension and individual alpha frequency. *Experimental Psychology*, *51*(4), 279–289. https://doi.org/10.1027/1618-3169.51.4.279

Bornkessel-Schlesewsky, I., Philipp, M., Alday, P. M., Kretzschmar, F., Grewe, T., Gumpert, M., … Schlesewsky, M. (2015). Age-related changes in predictive capacity versus internal model adaptability: Electrophysiological evidence that individual differences outweigh effects of age. *Frontiers in Aging Neuroscience*, *7*(217). https://doi.org/10.3389/fnagi.2015.00217

Bromba, M. U. A., & Ziegler, H. (1981). Application hints for Savitzky-Golay digital smoothing filters. *Analytical Chemistry*, *53* (11), 1583–1586. https://doi.org/10.1021/ac00234a011

Cecere, R., Rees, G., & Romei, V. (2015). Individual differences in alpha frequency drive crossmodal illusory perception. *Current Biology*, *25*(2), 231–235. https://doi.org/10.1016/j.cub.2014.11.034

Chen, A. C. N., Feng, W., Zhao, H., Yin, Y., & Wang, P. (2008). EEG default mode network in the human brain: Spectral regional field powers. *NeuroImage*, *41*(2), 561–574. https://doi.org/10.1016/j.neuroimage.2007.12.064

Chiang, A. K. I., Rennie, C. J., Robinson, P. A., Roberts, J. A., Rigozzi, M. K., Whitehouse, R. W., … Gordon, E. (2008). Automated characterization of multiple alpha peaks in multi-site

electroencephalograms. *Journal of Neuroscience Methods*, *168*(2), 396–411. https://doi.org/10.1016/j.jneumeth.2007.11.001

Chiang, A. K. I., Rennie, C. J., Robinson, P. A., van Albada, S. J., & Kerr, C. C. (2011). Age trends and sex differences of alpha rhythms including split alpha peaks. *Clinical Neurophysiology*, *122*(8), 1505–1517. https://doi.org/10.1016/j.clinph.2011.01.040

Cohen, M. X. (2017). Rigor and replication in time-frequency analyses of cognitive electrophysiology data. *International Journal of Psychophysiology*, *111*, 80–87. https://doi.org/10.1016/j.ijpsycho.2016.02.001

Delorme, A., & Makeig, S. (2004). EEGLAB: An open source toolbox for analysis of single-trial EEG dynamics including independent component analysis. *Journal of Neuroscience Methods*, *134*(1), 9–21. https://doi.org/10.1016/j.jneumeth.2003.10.009

Dustman, R. E., Shearer, D. E., & Emmerson, R. Y. (1999). Life-span changes in EEG spectral amplitude, amplitude variability and mean frequency. *Clinical Neurophysiology*, *110*(8), 1399–1409. https://doi.org/10.1016/s1388-2457(99)00102-9

Gaál, Z. A., Boha, R., Stam, C. J., & Molnár, M. (2010). Age-dependent features of EEG-reactivity—Spectral, complexity, and network characteristics. *Neuroscience Letters*, *479*(1), 79–84. https://doi.org/10.1016/j.neulet.2010.05.037

Gasser, T., Bächer, P., & Steinberg, H. (1985). Test-retest reliability of spectral parameters of the EEG. *Electroencephalography & Clinical Neurophysiology*, *60*(4), 312–319. https://doi.org/10.1016/0013-4694(85)90005-7

Goljahani, A., D'Avanzo, C., Schiff, S., Amodio, P., Bisiacchi, P., & Sparacino, G. (2012). A novel method for the determination of the EEG individual alpha frequency. *NeuroImage*, *60*(1), 774–786. https://doi.org/10.1016/j.neuroimage.2011.12.001

Grandy, T. H., Werkle-Bergner, M., Chicherio, C., Lövdén, M., Schmiedek, F., & Lindenberger, U. (2013). Individual alpha peak frequency is related to latent factors of general cognitive abilities. *NeuroImage*, *79*, 10–18. https://doi.org/10.1016/j.neuroimage.2013.04.059

Grandy, T. H., Werkle-Bergner, M., Chicherio, C., Schmiedek, F., Lövdén, M., & Lindenberger, U. (2013). Peak individual alpha frequency qualifies as a stable neurophysiological trait marker in healthy younger and older adults. *Psychophysiology*, *50*(6), 570–582. https://doi.org/10.1111/psyp.12043

Gulbinaite, R., Ilhan, B., & VanRullen, R. (2017). The triple-flash illusion reveals a driving role of alpha-band reverberations in visual perception. *Journal of Neuroscience*, *37*(30), 7219–7230. https://doi.org/10.1523/jneurosci.3929-16.2017

Gulbinaite, R., van Viegen, T., Wieling, M., Cohen, M. X., & VanRullen, R. (2017). Individual alpha peak frequency predicts 10 Hz flicker effects on selective attention. *Journal of Neuroscience*, *37*(42), 10173–10184. https://doi.org/10.1523/jneurosci.1163-17.2017

Haegens, S., Cousijn, H., Wallis, G., Harrison, P. J., & Nobre, A. C. (2014). Inter- and intra-individual variability in alpha peak frequency. *NeuroImage*, *92*, 46–55. https://doi.org/10.1016/j.neuroimage.2014.01.049

Hedden, T., & Gabrieli, J. D. E. (2004). Insights into the ageing mind: A view from cognitive neuroscience. *Nature Reviews Neuroscience*, *5*(2), 87–96. https://doi.org/10.1038/nrn1323

Hülsdünker, T., Mierau, A., & Strüder, H. K. (2016). Higher balance task demands are associated with an increase in individual alpha peak frequency. *Frontiers in Human Neurosciences*, *9*, 695. https://doi.org/10.3389/fnhum.2015.00695

Jann, K., Koenig, T., Dierks, T., Boesch, C., & Federspiel, A. (2010). Association of individual resting state EEG alpha frequency and cerebral blood flow. *NeuroImage*, *51*(1), 365–372. https://doi.org/10.1016/j.neuroimage.2010.02.024

Klimesch, W. (1997). EEG-alpha rhythms and memory processes. *International Journal of Psychophysiology*, *26*, 319–340. https://doi.org/10.1016/s0167-8760(97)00773-3

Klimesch, W. (1999). EEG alpha and theta oscillations reflect cognitive and memory performance: A review and analysis. *Brain Research Reviews*, *29*(2–3), 169–195. https://doi.org/10.1016/s0165-0173(98)00056-3

Klimesch, W. (2012). Alpha-band oscillations, attention, and controlled access to stored information. *Trends in Cognitive Sciences*, *16*(12), 606–617. https://doi.org/10.1016/j.tics.2012.10.007

Klimesch, W., Doppelmayr, M., & Hanslmayr, S. (2006). Upper alpha ERD and absolute power: Their meaning for memory performance. In C. Neuper & W. Klimesch (Eds.), *Event-related dynamics of brain oscillations* (Vol. *159*, pp. 151–165). Amsterdam, The Netherlands: Elsevier Science BV. https://doi.org/10.1016/s0079-6123(06)59010-7

Klimesch, W., Doppelmayr, M., Schimke, H., & Pachinger, T. (1996). Alpha frequency, reaction time, and the speed of processing information. *Journal of Clinical Neurophysiology*, *13*(6), 511–518. https://doi.org/10.1097/00004691-199611000-00006

Klimesch, W., Schimke, H., Ladurner, G., & Pfurtscheller, G. (1990). Alpha frequency and memory performance. *Journal of Psychophysiology*, *4*, 381–390.

Klimesch, W., Schimke, H., & Pfurtscheller, G. (1993). Alpha frequency, cognitive load and memory performance. *Brain Topography*, *5*(3), 241–251. https://doi.org/10.1007/bf01128991

Kondacs, A., & Szabo, M. (1999). Long-term intra-individual variability of the background EEG in normals. *Clinical Neurophysiology*, *110*(10), 1708–1716. https://doi.org/10.1016/s1388-2457(99)00122-4

Köpruner, V., Pfurtscheller, G., & Auer, L. M. (1984). Quantitative EEG in normals and in patients with cerebral ischemia. *Progress in Brain Research*, *62*, 29–50. https://doi.org/10.1016/s0079-6123(08)62168-8

Kreitman, N., & Shaw, J. C. (1965). Experimental enhancement of alpha activity. *Electroencephalography & Clinical Neurophysiology*, *18*(2), 147–155. https://doi.org/10.1016/0013-4694(65)90021-0

Lodder, S. S., & van Putten, M. J. A. M. (2011). Automated EEG analysis: Characterizing the posterior dominant rhythm. *Journal of Neuroscience Methods*, *200*(1), 86–93. https://doi.org/10.1016/j.jneumeth.2011.06.008

Luo, J., Ying, K., He, P., & Bai, J. (2005). Properties of Savitzky-Golay digital differentiators. *Digital Signal Processing*, *15*(2), 122–136. https://doi.org/10.1016/j.dsp.2004.09.008

Lykken, D. T., Tellegen, A., & Thorkelson, K. (1974). Genetic determination of EEG frequency spectra. *Biological Psychology*, *1*, 245–259. https://doi.org/10.1016/0301-0511(74)90001-5

Malone, S. M., Burwell, S. J., Vaidyanathan, U., Miller, M. B., McGue, M., & Iacono, W. G. (2014). Heritability and molecular-genetic basis of resting EEG activity: A genome-wide association study. *Psychophysiology*, *51*(12), 1225–1245. https://doi.org/10.1111/psyp.12344

Milton, A. & Pleydell-Pearce, C. (2017). Exploring the relationship of phase and peak-frequency EEG alpha-band and beta-band activity to temporal judgments of stimulus duration. *Cognitive Neuroscience*, *8*(4), 193–205. https://doi.org/10.1080/17588928.2017.1359524

Näpflin, M., Wildi, M., & Sarnthein, J. (2007). Test-retest reliability of resting EEG spectra validates a statistical signature of persons. *Clinical Neurophysiology*, *118*(11), 2519–2524. https://doi.org/10.1016/j.clinph.2007.07.022

Noachtar, S., Binnie, C., Ebersole, J., Mauguière, F., Sakamoto, A., & Westmoreland, B. (2004). A glossary of terms most commonly used by clinical electroencephalographers and proposal for the report form for the EEG findings. *Klinische Neurophysiologie*, *35*(1), 5–21. https://doi.org/10.1055/s-2003-812583

Oldfield, R. C. (1971). The assessment and analysis of handedness: The Edinburgh inventory. *Neuropsychologia*, *9*, 97–113. https://doi.org/10.1016/0028-3932(71)90067-4

Press, W. H., Teukolsky, S. A., Vetterling, W. T., & Flannery, B. P. (1992). *Numerical recipes in Fortran 77: The art of scientific computing*. (2nd ed., vol. *1*). New York, NY: Cambridge University Press.

Pritchard, W. S. (1992). The brain in fractal time: 1/f-like power spectrum scaling of the human electroencephalogram. *International Journal of Neuroscience*, *66*(1–2), 119–129. https://doi.org/10.3109/00207459208999796

Rihs, T. A., Michel, C. M., & Thut, G. (2007). Mechanisms of selective inhibition in visual spatial attention are indexed by alpha-band EEG synchronization. *European Journal of Neuroscience*, *25*(2), 603–610. https://doi.org/10.1111/j.1460-9568.2007.05278.x

Salthouse, T. A. (2011). Neuroanatomical substrates of age-related cognitive decline. *Psychological Bulletin*, *137*(5), 753–784. https://doi.org/10.1037/a0023262

Samaha, J., & Postle, B. R. (2015). The speed of alpha-band oscillations predicts the temporal resolution of visual perception. *Current Biology*, *25*(22), 2985–2990. https://doi.org/10.1016/j.cub.2015.10.007

Savitzky, A., & Golay, M. J. E. (1964). Smoothing and differentiation of data by simplified least squares procedures. *Analytical Chemistry*, *36*(8), 1627–1639. https://doi.org/10.1021/ac60214a047

Schafer, R. W. (2011). What is a Savitzky-Golay filter? *IEEE Signal Processing Magazine*, *28*(4), 111–117. https://doi.org/10.1109/msp.2011.941097

Smit, C. M., Wright, M. J., Hansell, N. K., Geffen, G. M., & Martin, N. G. (2006). Genetic variation of individual alpha frequency (IAF) and alpha power in a large adolescent twin sample. *International Journal of Psychophysiology*, *61*(2), 235–243. https://doi.org/10.1016/j.ijpsycho.2005.10.004

Surwillo, W. W. (1961). Frequency of the 'alpha' rhythm, reaction time and age. *Nature*, *191*(4790), 823–824. https://doi.org/10.1038/191823a0

Surwillo, W. W. (1963). The relation of simple response time to brain-wave frequency and the effects of age. *Electroencephalography & Clinical Neurophysiology*, *15*(1), 105–114. https://doi.org/10.1016/0013-4694(63)90043-9

van Albada, S. J., & Robinson, P. A. (2013). Relationships between electroencephalographic spectral peaks across frequency bands. *Frontiers in Human Neuroscience*, *7*(56), 1–18. https://doi.org/10.3389/fnhum.2013.00056

van der Meij, R., van Ede, F., & Maris, E. (2016). Rhythmic components in extracranial brain signals reveal multifaceted task modulation of overlapping neuronal activity. *PLOS One*, *11*(6), e0154881. https://doi.org/10.1371/journal.pone.0154881

Vogel, W., & Broverman, D. M. (1964). Relationship between EEG and test intelligence: A critical review. *Psychological Bulletin*, *62*(2), 132–144. https://doi.org/10.1037/h0049067

Welch, P. D. (1967). The use of fast Fourier transform for the estimation of power spectra: A method based on time averaging over short, modified periodograms. *IEEE Transactions on Audio and Electroacoustics*, *AU15*(2), 70–73. https://doi.org/10.1109/tau.1967.1161901

Ziegler, H. (1981). Properties of digital smoothing polynomial (DISPO) filters. *Applied Spectroscopy*, *35*(1), 88–92. https://doi.org/10.1366/0003702814731798

SUPPORTING INFORMATION

Additional Supporting Information may be found online in the supporting information tab for this article.

Appendix S1
Table S1
Figure S1
Figure S2

How to cite this article: Corcoran AW, Alday PM, Schlesewsky M, Bornkessel-Schlesewsky I. Toward a reliable, automated method of individual alpha frequency (IAF) quantification. *Psychophysiology*. 2018; e13064. https://doi.org/10.1111/psyp.13064

APPENDIX

This appendix gives a more formal account of the estimators implemented in the algorithm.

Peak alpha frequency

Peak alpha frequency (PAF) can be formalized in terms of the local maximum within the alpha band:

$$\mathrm{PAF}=\begin{cases}\arg\max\limits_{f\in\text{alpha band}}\mathrm{PSD}(f), & \mathrm{PSD}(f)-\mathrm{PSD}(f')\geq\varphi\ \forall f'\neq f\\ \text{undefined}, & \text{otherwise}\end{cases} \tag{1}$$

where argmax returns the frequency bin (or subset of bins) f containing the maximal power value maxPSD(f) registered within the set of frequency bins spanning the alpha band. Note that, for the output of arg max to qualify as an estimate of PAF, it must return a single frequency bin f with a corresponding power spectral density $\geq \varphi$, where φ defines the minimum threshold value differentiating a substantive spectral peak from background noise.

First- and second-derivative tests

Derivatives describe the relative rate of change in the dependent variable or function $g(x)$ given some value of the independent variable x. The first derivative of a vector of PSD estimates thus provides point estimates of the (instantaneous) rate of change in the amount of spectral power estimated for each frequency bin resolved in the analysis. This relationship can be formalized as

$$g'(x)=\lim_{\Delta x\to 0}\frac{\Delta g(x)}{\Delta x}, \tag{2}$$

where $g'(x)$ is the first derivative of the relative change in the power estimate $g(x)$ at frequency bin x.

Another way to conceptualize this relationship is to construe the derivative as describing the slope of the tangent line to the PSD function $g(x)$ at any given frequency bin x. From this perspective, it becomes clear that the first derivative will be zero (i.e., the slope of the tangent will be horizontal) at any point in the function corresponding to a peak or trough. In the case of the former, the derivative will change from a positive value (as the function ascends toward its peak) to a negative value (once the function begins to descend) as the tangent traverses the local maximum. As such, positive-to-negative sign changes (i.e., downward-going zero crossings) within the first derivative offer a convenient index of local maxima. Conversely, sign changes in the opposite direction (i.e., upward-going zero crossings) can likewise be used to identify local minima.[1]

The second derivative of the PSD is derived by differentiating the first derivative:

$$g''(x)=\lim_{\Delta x\to 0}\frac{\Delta g'(x)}{\Delta x}, \tag{3}$$

where $g''(x)$ is the derivative of the first derivative $g'(x)$ at frequency bin x. In other words, the second derivative is simply the rate of change of the first derivative of some function $g(x)$. Second derivatives are useful for evaluating whether the curvature of a function is concave up (i.e., convex) or concave down at any given value of x. The transition of a curve's direction between concave up and concave down is characterized by an inflection point, which registers a second derivative value of zero. Consequently, inflection points can be identified by applying the same zero-crossing procedure described for locating optima in the first derivative.

Quantifying peak quality

Having defined both the height and width of the putative alpha peak by means of the first- and second-derivative test, relative peak quality is quantified as

$$Q=\frac{\int_{i_1}^{i_2}\mathrm{PSD}(f)\ df}{i_2-i_1}, \tag{4}$$

where Q is the scaled average power within the peak interval $[i_1, i_2]$.[2] (In a very strict sense, Q is the mean value of the power spectral density function on the peak interval as given by the mean value theorem.) Note that the inclusion of the denominator ensures that spectral width is taken into account when calculating Q.

Center of gravity

The center of gravity (CoG) is the PSD-weighted mean alpha frequency, which can be expressed as

$$\mathrm{CoG}=\frac{\int_{f_1}^{f_2}\mathrm{PSD}(f)\cdot f\ df}{\int_{f_1}^{f_2}\mathrm{PSD}(f)\ df}, \tag{5}$$

where f_1 and f_2 index the frequency bins bounding the alpha-band interval.

[1] A lack of sign change (e.g., a positive derivative going to zero and then becoming strictly positive again) corresponds to a plateau.

[2] Notice that the interval bounded by $[i_1, i_2]$ is distinct from that bounded by $[f_1, f_2]$, the estimated span of the individualized alpha-band window. The former yields a narrower frequency range than the latter, and does not take into account secondary peaks within the alpha band.

CoG calculation follows the standard procedure described by Klimesch and colleagues (1990, 1993), with the exception that the bounds of each channel's alpha interval are detected automatically. The analysis routine derives these bounds by taking the left- and right-most peaks within W_α (i.e., those peaks in the lowest and highest frequency bins, respectively; these may coincide with the PAF), and searching the first derivative for evidence of the nearest local minimum (a) prior to the left-most peak (f_1), and (b) following the right-most peak (f_2).[3] Since some spectra show a relatively shallow roll-off as the edges of the alpha peak diminish, and thus do not culminate in a local minimum for several frequency bins away from the main body of the component structure, we relaxed the requirement for an upward-going zero crossing (i.e., evidence of a local minimum) such that the transition into a prolonged shallow gradient is taken as sufficient evidence of the individual alpha bounds f_1 or f_2. This criterion was formalized as

$$f_1 = \arg\max_{f<\mathrm{PAF}} |PSD'(f)| < 1, \tag{6}$$

$$f_2 = \arg\min_{f>\mathrm{PAF}} |PSD'(f)| < 1. \tag{7}$$

f_1 and f_2 estimates from each eligible channel are averaged to yield the individualized alpha-band window. This window defines the index of summation (i.e., frequency band coverage) used to calculate the CoG across all available channels.

Summary statistics

If a sufficient number of channels (as stipulated by *cMin*) furnish PAF and individualized alpha window estimates, channel PAF and CoG estimates are averaged to generate IAF summary statistics. Mean PAF (PAF_M) is a weighted average that takes into account the Q values associated with each peak estimate:

$$\mathrm{PAF}_M = \frac{\sum_{c=1}^{C} \mathrm{PAF}_c \cdot \lambda_c}{\sum_{c=1}^{C} \lambda_c}, \tag{8}$$

where c identifies the channel drawn from the set of all available channels C, and λ_c is the channel weighting derived by dividing Q_c by the maximum Q_c in C (such that $\sum \lambda_c = 1$). In contrast to PAF_M, all CoG channel estimates contribute equally to the calculation of mean CoG (CoG_M). If there are an insufficient number of channel estimates to satisfy *cMin*, no PAF_M or CoG_M estimates are returned (in some cases, *cMin* will be satisfied for CoG_M, but not PAF_M, on account of the latter's more stringent criteria).

Since pre-/postexperiment recordings may not be equivalent in terms of quantity of information rendered, grand-averaged IAF estimates (IAF_{GA}) are calculated using a weighted mean that takes into account the proportion of channels that contributed to each constituent summary statistic:

$$\mathrm{IAF}_{GA} = \frac{\mathrm{IAF}_1\beta_1 + \mathrm{IAF}_2\beta_2}{\beta_1 + \beta_2}, \tag{9}$$

where either PAF or CoG are substituted in place of IAF, β constitutes the weighting afforded to the channelwise mean estimates derived from each recording, and subscript indices indicate the identity of the EEG recording. For PAF estimates, β is the number of channels used to estimate PAF_M divided by total number of channels included in the analysis. For CoG estimates, β is the number of channels used to estimate the mean individualized alpha-band window divided by total number of channels included in the analysis.

[3]This contingency allows for the individualized alpha-band window, and thus the CoG, to be estimated even in cases where there is no clear PAF (e.g., in the presence of split peaks).